A two-magnet strategy for improved mixing and capture from biofluids

Thomas F. Scherr, Hayley B. Ryskoski, Andrew B. Doyle,
and Frederick R. Haselton
Department of Biomedical Engineering, Vanderbilt University, Nashville, Tennessee 37235, USA

(Received 19 January 2016; accepted 30 March 2016; published online 11 April 2016)

Magnetic beads are a popular method for concentrating biomolecules from solution and have been more recently used in multistep pre-arrayed microfluidic cartridges. Typical processing strategies rely on a single magnet, resulting in a tight cluster of beads and requiring long incubation times to achieve high capture efficiencies, especially in highly viscous patient samples. This report describes a two-magnet strategy to improve the interaction of the bead surface with the surrounding fluid inside of a pre-arrayed, self-contained assay-in-a-tube. In the two-magnet system, target biomarker capture occurs at a rate three times faster than the single-magnet system. In clinically relevant biomatrices, we find a 2.5-fold improvement in biomarker capture at lower sample viscosities with the two-magnet system. In addition, we observe a 20% increase in the amount of protein captured at high viscosity for the two-magnet configuration relative to the single magnet approach. The two-magnet approach offers a means to achieve higher biomolecule extraction yields and shorter assay times in magnetic capture assays and in self-contained processor designs. *Published by AIP Publishing*. [http://dx.doi.org/10.1063/1.4946014]

I. INTRODUCTION

Magnetic beads are a simple substrate for benchtop biomolecule isolation and extraction.[1–3] Flow-through systems deliver magnetic particles via carrier fluid motion, where magnetic beads are suspended in a fluid and captured by a magnetic field.[4–10] To overcome the challenges inherent in fluid-based delivery of magnetic beads, an alternative technology based on static pre-arrayed fluid cartridges has been developed where magnetic beads are again used as a mobile substrate, but transported by magnetic entrainment rather than bulk fluid flow. In these designs, each chamber is used to perform a single processing or reaction step and instead of pumping different fluids past immobilized ligands, surface-functionalized magnetic beads are carried by a magnetic field from fluid chamber to fluid chamber.[11–17] These devices typically consist of fluids contained in processing or reaction chambers separated from one another by an immiscible fluid.[18–22] There are several advantages to the pre-arrayed configuration for medical diagnostics. First, the solutions and their concentrations are controlled during fabrication, and they remain unchanged during operation. Second, the entire pre-arrayed cassette can be made as a closed system, which limits contamination and hazardous exposure. Third, the liquid locations in pre-arrayed cassettes are at known, reproducible locations, which give them a straightforward end-user work flow[12,23] and the potential for simple automated processing.[18,24–26] These benefits position microfluidic pre-arrayed cartridges for use as ready-made, "off-the-shelf" assays for biomolecule capture and extraction.

We have previously described a sample preparation approach for diagnostic applications that relies on a series of pre-arrayed processing solutions separated by immiscible "surface tension-valves" in an enclosed tube format. The underlying characteristics of these valves have been studied in detail, and optimal performance parameters have been identified.[27] The tube format has been demonstrated as a method for tuberculosis DNA extraction and amplification,

protein isolation for malaria detection, cell counting for human immunodeficiency virus diagnosis, and clinical chemistry assays.[21,22,27–29] In each of these assays, a single magnet was moved relative to the length of the tube to transfer the magnetic beads across the immiscible fluid interface and into the sequential processing chambers. We have recently described a two-magnet design for processing which worked particularly well for viscous sputum samples used for tuberculosis diagnosis.[18] In this case, the presence of a second magnet, with no other mixing motions, appeared to be critical for successful DNA isolation.

This report provides a detailed comparison of how the inclusion of a second magnet improves bead-fluid interactions for a range of patient sample types and viscosities. We demonstrate enhanced dispersion of magnetic beads inside of a small diameter length of tubing using only relative motion between the tube and a pair of magnets. The addition of a second magnet creates a symmetric magnetic field, in both the transverse and axial planes of the tube, which avoids a "lumped" cluster of beads against the tube wall, as well as maintains bead transfer across the surface tension valves. In this approach, we also utilize a high-speed relative motion to place the magnetic beads in a magnetic field with large dispersive forces, rather than the concentrating forces seen with a single magnet. We then test our hypothesis that magnetic dispersion of beads during the initial binding step results in more rapid capture of biomarkers to beads and, hence, shorter assay times.

II. METHODS

A. Theory and numerical analysis

Magnetic forces exerted on beads and bead spatial distributions were analyzed with a commercial finite-element package (COMSOL Multiphysics v5.0, Burlington, MA). The two-dimensional circular simulation domain, of radius 100 mm, consisted of a rectangle representing a tube (100 mm height × 3 mm width), and either one or two cylinder magnets (projected as 0.25 in. radius circles when placed perpendicular to the tubing). The theory behind magnetic fields due to permanent magnets is well-established and provided in detail in the Appendix. After the solution of the static magnetic field, the force per volume that results on magnetic beads was calculated from

$$\mathbf{F_m} = \frac{\chi}{\mu_0}(\mathbf{B}\cdot\nabla)\mathbf{B}. \tag{1}$$

To predict magnetic bead distributions that result from these forces, the mixture model was used to model the magnetic beads as a particulate suspension. The mixture model, as developed by others,[30,31] is briefly outlined here. The continuity equation, the conservation of momentum, and the solid phase species transport equations are

$$(\rho_f - \rho_s)[\nabla\cdot(\phi_s(1-c_s)\mathbf{u_{slip}})] + \rho_f(\nabla\cdot\mathbf{u}) = 0, \tag{2}$$

$$\rho\frac{\partial\mathbf{u}}{\partial t} + \rho(\mathbf{u}\cdot\nabla)\mathbf{u} = -\nabla\mathrm{p} - \nabla\cdot\left(\rho c_s(1-c_s)\mathbf{u_{slip}}\mathbf{u_{slip}}\right) + \nabla\cdot\left[\eta(\nabla\mathbf{u}+\nabla\mathbf{u}^T)\right] + \rho\mathbf{g} + \mathbf{F_{body}}, \tag{3}$$

$$\frac{\partial\phi_s}{\partial t} + \nabla\cdot\left(\phi_s\mathbf{u} + \phi_s(1-c_s)\mathbf{u_{slip}}\right) = 0. \tag{4}$$

In these equations, $\mathbf{u}$ is the mass-averaged mixture velocity, c_s is the particulate mass fraction, $\mathbf{u_{slip}}$ is the relative velocity between the solid and liquid phases, Φ_s is the solid phase volume fraction, ρ is the volume weighted mixture density, and η is the mixture viscosity. The mixture viscosity follows a Kreiger-type expression, where the viscosity is dependent on the local solid phase fraction. The magnetic bead force from Eq. (1) was multiplied by the local volume fraction of the magnetic beads and included in the model as a body force on the discrete phase (magnetic beads) only. In the mixture model, the tubing walls were given no slip boundary conditions and zero dispersed phase flux. The fluid was initially at rest throughout the entire tube

domain. The volume fraction of the dispersed phase was set to zero throughout the tube, with the exception of three "seed" locations. These seed locations were created as 1.5 mm diameter circles, at the center of the tube and 6 mm away in both directions from the center, with a specified initial dispersed phase volume fraction of 0.4. The transient simulations were run from 0 to 3 s, which was sufficient time to reach a stable magnetic bead distribution.

B. Rheology of biofluids

Stress-strain measurements of biofluids were made on a Brookfield DV-II+ Pro (Brookfield, Middleboro, MA) cone-plate viscometer with a SP-40 spindle. A sample volume of 500 μl for each of the following was used: pooled Human blood (BioreclamationIVT, Hicksville, NY), pooled Human serum (BioreclamationIVT, Hicksville, NY), pooled Human saliva (Lee Biosolutions, Maryland Heights, MO), a synthetic sputum analog (made according to literature[32]), and phosphate buffered saline (PBS) with 0.1% Tween (PBST). In addition, measurements were made for each of the above biofluids at a 1:1 (v/v) dilution with PBST. All biofluid samples were allowed sufficient time to reach room temperature, and all viscometer measurements were made at room temperature. In blood, serum, and saliva, measurements were made at discrete shear rates of 7.5 s^{-1}, 18.8 s^{-1}, 37.5 s^{-1}, 75 s^{-1}, 150 s^{-1}, and 375 s^{-1}. To remain within instrument torque tolerances, the following adjustments were made for sputum and 50% sputum: sputum measurements were made at 2.25 s^{-1}, 3.75 s^{-1}, 4.5 s^{-1}, 7.5 s^{-1}, and 11.3 s^{-1}; 50% sputum measurements were made at 4.5 s^{-1}, 7.5 s^{-1}, 11.3 s^{-1}, 18.8 s^{-1}, 37.5 s^{-1}, and 75 s^{-1}. All samples were measured in triplicate. Stress-strain measurements for each fluid were fit to the power-law function

$$\tau = K\dot{\gamma}^n. \tag{5}$$

Apparent viscosities were determined as a function of shear rate through

$$\mu_{eff} = K|\dot{\gamma}|^{n-1}. \tag{6}$$

Using the apparent viscosity calculated in Eq. (6), molecular diffusivities were estimated from the Stokes-Einstein equation

$$D_{ab} = \frac{k_B T}{6\pi\mu_{eff} R_H}, \tag{7}$$

where k_B is the Boltzmann constant, T is the temperature, and R_H is the hydrodynamic radius of the molecule diffusing in a fluid with viscosity of μ_{eff}.

C. Assay tube preparation

The enclosed assay tube system consists of a small diameter section of tubing, which holds a series of preloaded solutions separated by surface tension valves to concentrate and elute Histidine-tagged green fluorescent protein (HGFP) with Cobalt-nitrilotriacetic acid (NTA) surface functionalized magnetic beads. We envision these tubes as pre-prepared cassettes that could be made available for "off-the-shelf" use. The assay tube, an 8 in. portion of 0.093 in. ID fluorinated ethylene propylene (FEP) tubing (#9369T24, McMaster Carr, Atlanta, GA), was long enough to run through the positioning rollers and magnet holder (Figure 1). The bead chamber solution, which consists of 800 μg of Dynabeads His-Tag Isolation & Pulldown (Life Technologies Corporation, Grand Island, NY) mixed with 100 μl of phosphate buffered saline and 0.1% Tween-20 (PBST), was first loaded into the FEP tubing, followed by 100 μl of air. This air chamber separates the sequential liquid chambers by approximately 0.75 in. From our previous work, we have found this distance to be large enough to maintain stable separation, while still enabling reproducible magnetic bead transfer from chamber to chamber. Before use, the magnetic beads were settled by gravity and collected at the bottom of the bead chamber. The force due to gravity alone is not sufficient for the magnetic beads to overcome the

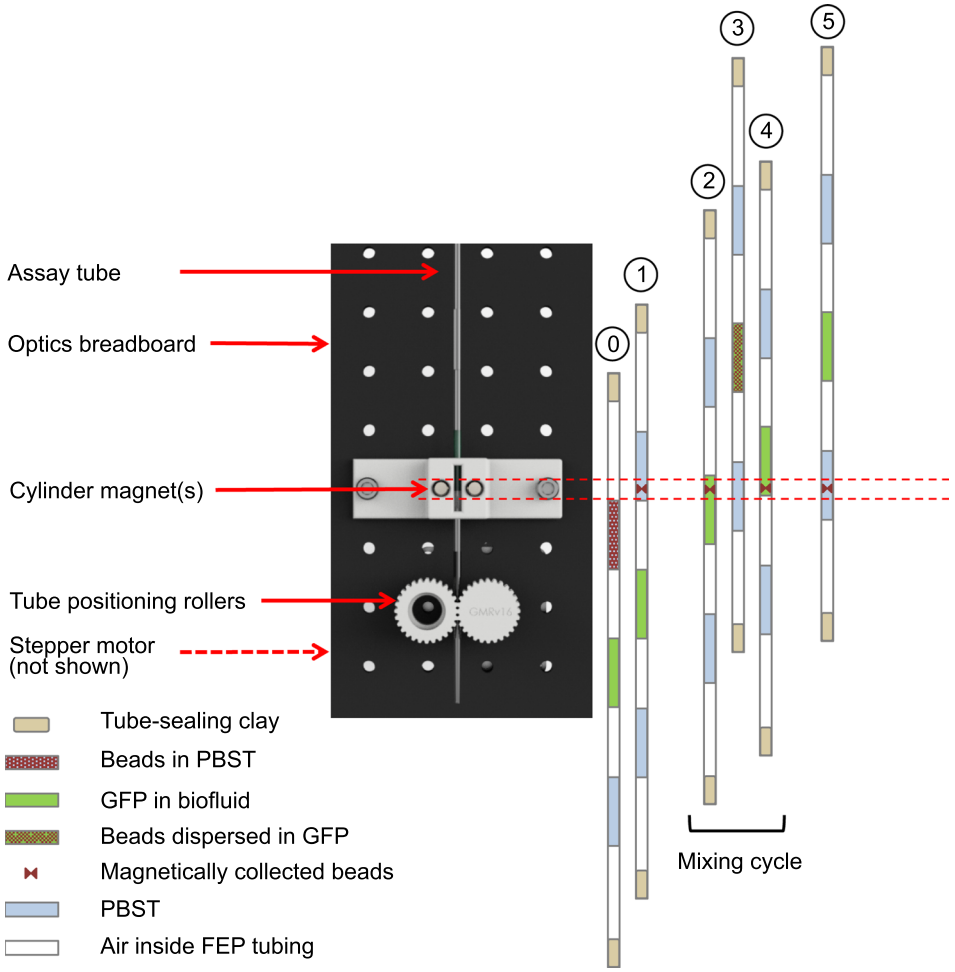

FIG. 1. The magnetic mixing experimental setup (left) and the six steps in the tube motion profile (right).

interfacial tension at the liquid/air interface, and hence the beads remain in their original chamber. Next came the target analyte chamber, which contained 50 μl of 0.1 mg/ml HGFP (#ab134853, Abcam Inc., Cambridge, MA) in 50 μl of either PBST or biofluid; the analyte chamber was again followed by 100 μl volume of air. Last, the final processing chamber, which consisted of 100 μl of PBST, was loaded into the tube. The three chambers were then centered in the tube by adding additional air to move the chambers down the length of the tube, and the tube was sealed with clay.

D. Qualitative tube imaging

A Nikon D800 camera equipped with a Nikon AF-S VR Micro-NIKKOR 105 mm f/2.8 G IF-ED lens was used to take photographs of the magnetic beads inside of stationary and moving tubes for qualitative comparison between the single and two magnet configurations. For imaging, 800 μg of beads were initially combined with 100 μl of PBST in one chamber of the tube and imaged during the tube motion.

E. Automated biomarker extraction in tube

A schematic of the automated extraction experimental setup is shown in Figure 1. The assay tube was threaded between 3D printed (ProJet 3510 HD Plus, 3D Systems, Rock Hill, SC) positioning rollers and a 3D printed magnet holder, with the magnetic bead chamber first.

The magnet holder had either one or two diametrically magnetized cylindrical magnets (#D48DIA, K&J Magnetics, Pipersville, PA), located 1 mm away from the side of the tube. With a single magnet, the north pole was perpendicular to the tube; with two magnets, one magnet's north pole was perpendicular to the tube, while the opposite magnet's south pole was perpendicular to the tube. Since the two magnets are magnetically attracted to one another, their angular position was stable and the poles remain in place. The tube was positioned so that the top of the bead chamber was at the intersection of the positioning rollers. A stepper motor with 20 000 steps per revolution (Applied Motion Products, Watsonville, CA) was controlled through an ST5-Q stepper motor driver (Applied Motion Products, Watsonville, CA), with commands generated using the Q Programmer software (Applied Motion Products, Watsonville, CA). The shaft of the motor was press-fit to one of the custom positioning rollers, which was used to turn the other roller and drive the assay tube. To collect the beads and move them from the first to second chamber, the tube was moved at a velocity of 0.35 mm/s by setting the motor to a velocity of 0.005 rps. This speed was used as the beads were slowly pulled through the first chamber and first surface tension valve and into the bottom of the target analyte chamber. During this slow tube movement, the magnetic beads remained stationary while the assay tube moved. Since the magnetic beads are engaged with the magnet, we refer to this speed as the "magnet-engaged speed." At this point, the tube was rapidly pulled down at a linear speed of 90.7 mm/s, by setting the motor to 10 rps. This generates a strong drag force on the magnetic beads that is greater than the magnetic force, and as such the magnetic beads are no longer held in place by the magnet. In particular, this "magnet-disengaged speed" is responsible for dispersing the beads throughout the HGFP chamber. After a 1 s wait time, the tube was pulled up at the magnet-engaged speed to recollect the beads and move them to the bottom of the HGFP chamber. This magnet-disengaged motion for dispersion, followed by a magnet-engaged motion for re-gathering the beads at the bottom of the HGFP chamber, was repeated for 1, 5, 10, 15, 20, and 25 cycles to vary the number of times the beads were dispersed throughout the HGFP. Finally, the tube was pulled down at the magnet-engaged speed into the third fluid chamber containing PBST. The magnets were removed from the apparatus, and the tube was manually removed through the top of the magnet holder.

F. Bead and HGFP quantification

Following biomarker extraction, the assay tube was cut to preserve the contents of each chamber in separate microcentrifuge tubes and quantify the amounts of magnetic beads and HGFP in each. The tubes were placed in a centrifuge for 3 min at a speed of 14 000 rpm and then set on a magnetic separator. The supernatant was removed from each tube, and the fluorescence of the supernatant from chambers 2 and 3 were measured at 510 nm using a 3 μl aliquot on a ND-3300 spectrofluorometer (Nanodrop, Wilmington, DE). Next, 100 μl of 500 mM imidazole in PBS was added to the beads remaining in the tubes from chambers 2 and 3, and each were vortexed for 30 s to elute the HGFP captured on the surface of the beads. The tubes were again placed in a centrifuge for 3 min at a speed of 14 000 rpm and then set on a magnetic separator. The supernatant was removed from the tubes containing the contents of chambers 2 and 3, and the fluorescence of each was measured at 510 nm. After the removal of the supernatants, 100 μl of deionized water was added to the tubes containing the beads from chambers 1 and 2, and 600 μl was added to the tube containing the beads of chamber 3. The absorbance of each chamber was then measured, using a 3 μl aliquot, at 700 nm on a NanoDrop ND-1000 UV/Vis spectrophotometer (NanoDrop, Wilmington, DE).

G. Minimum and maximum mixing experiments

To determine the effect of pure molecular diffusion on the isolation of HGFP from the target analyte chamber, the assay tubes were prepared as described above with PBST as the biofluid analogue. The operating protocol of the automated extraction was modified as follows. The tube was moved at the magnet-engaged speed, carrying the beads from their initial chamber into the HGFP chamber. Once the beads reached the center of the HGFP chamber, the

motor motion was stopped. The beads remained held in this position for the equivalent residence time of a particular number of cycles (the assay times are shown in Table I). After this time, the tube was moved again at the magnet-engaged speed to move the beads from the HGFP chamber into the final chamber. The beads and HGFP were then analyzed as previously described.

To find an upper limit on the effect of uniform bead dispersion, maximum mixing experiments were carried out. Microcentrifuge tubes were loaded with 50 μl of 0.05 mg/ml HGFP in PBST and 800 μg of magnetic beads. The tubes were vortexed an equivalent residence time of 1, 5, 10, and 15 mixing cycles, as shown in Table I. After separation, the fluorescence of the supernatant was measured. HGFP bound to the surface of the beads was eluted with 500 mM imidazole, and the resulting fluorescence of the supernatant was measured.

H. Bulk fluid and bead transport

To analyze the bulk fluid that is carried over with the beads, an assay tube was prepared as described above with 1 mM fluorescein (Sigma-Aldrich, St. Louis, MO) in PBST in place of the HGFP. The tube was moved at the magnet-engaged speed carrying the magnetic beads from chamber 1 to chamber 3. MATLAB (v8.5, MathWorks, Natick, MA) was used to compare the bulk fluid transport and bead transport efficiency between the one- and two-magnet configurations with an unpaired, two-tailed Student's T-Test ($p < 0.05$).

III. RESULTS

A. Theory and qualitative imaging

The results of numerical simulations (Figure 2) show major differences in forces between the two magnetic configurations. In the single magnet configuration (Figure 2(a)), there are strong magnetic field gradients near the poles of the magnet that result in magnetic forces towards the tube wall at all locations. The magnitude of the magnetic force is strongest at the equator of the magnet. The force diagram in Figure 2(a) shows a concentrated magnetic field and large magnetic forces towards the magnet-side of the tube. As expected, the presence of a second magnet attracted to the first magnet alters the magnetic field considerably. With the second magnet present, there are strong forces towards the sides of the tubes, but there is zero magnetic force directly in between the two magnets (Figure 2(c)). Along the tube and farther away from the magnets, the magnetic forces are small but are pointed away from the magnets. This is a unique force field that is not seen with a single magnet; the magnetic force vector changes in magnitude but also in direction as the beads move through different positions in the magnetic field in the presence of two magnets. Viewed in the Lagrangian framework, the beads experience magnetic forces that vary in direction with changing position. It is this characteristic that enables a new field-driven mixing modality not possible with a single magnet.

The simulations also predict different spatial bead distributions for the two magnetic configurations. The beads are initialized to three seed locations, and after 3 s in the presence of a single magnet, the beads have formed a cluster along the tube wall (Figure 2(b)). After 3 s, the beads have reached a stable distribution, and little variation in bead distribution is seen. This follows the predicted magnetic force-field vectors from Figure 2(a). However, from the same

TABLE I. Residence times in the HGFP chamber and total assay times.

Number of cycles	Residence time in HGFP chamber (min)	Total assay time (min)
1	1	5
5	7	12
10	12	16
15	17	21
20	23	27
25	28	32

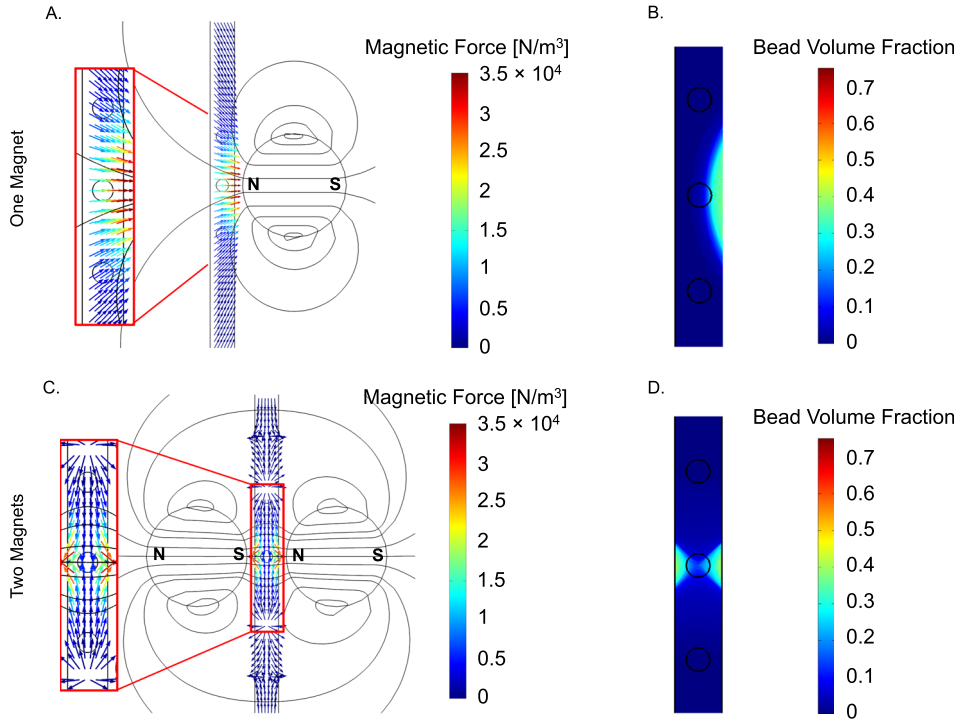

FIG. 2. Comparison of simulated magnetic field lines and simulated magnetic force vectors (force per volume) for (a) a single cylinder magnet and (c) two cylinder magnets. Mixture model spatial bead distributions at: (b) t = 3 s with one magnet and (d) t = 3 s with two magnets.

initial conditions but in the presence of a second magnet, the simulation predicts a horizontal hourglass bead distribution (Figure 2(d)) that is much different from the tightly packed cluster seen in the single magnet system (Figure 2(b)). Again, this distribution agrees with the predicted magnetic force field for this configuration.

The simulated bead distributions agree well with the experimental images of the bead distributions in stationary tubes (Figure 3). In these experiments, the beads were initially dispersed

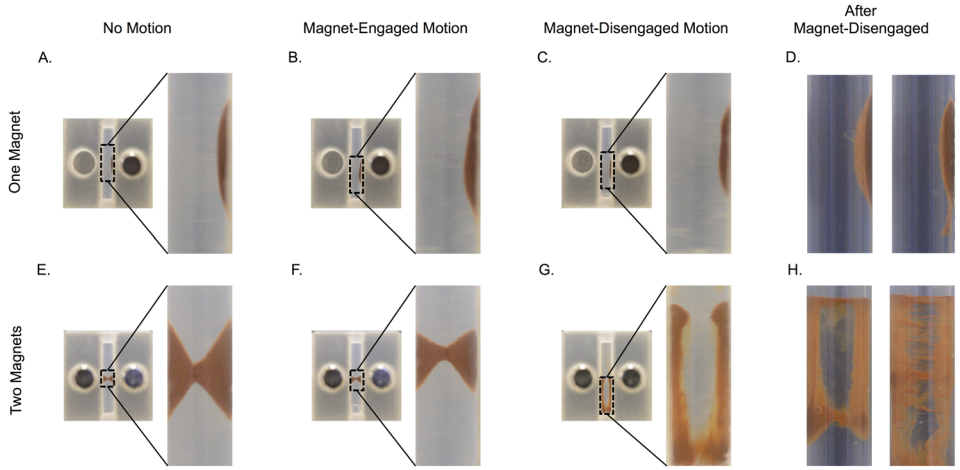

FIG. 3. Photographs of bead distributions with one magnet (a)–(d) and two magnets (e)–(h) under the following conditions: (a) and (e) bead distribution with no tube motion; (b) and (f) tube moving at the magnet-engaged speed; (c) and (g) tube moving at the magnet-disengaged speed; (d) and (h) (left) immediately after the tube was stopped after traveling at the magnet-disengaged speed; and (d) and (h) (right) 2 s after the tube was stopped after traveling at the magnet-disengaged speed. The magnets are out of the field of view of the camera in panels (d) and (h).

throughout the solution, and the tube was pulled past the magnets. Though the starting location of the beads in the experimental setup is different from the simulations, the beads still form the single cluster against the tube wall with the single magnet (Figure 3(a)) and the horizontal hourglass shape in the presence of two magnets (Figure 3(e)).

When the tube is in motion, as in Figures 3(b) and 3(f), the distribution of beads throughout the tube with two magnets instead of clustered along the wall with one magnet suggests the potential for improved fluid interaction in the two-magnet configuration. As the tube moves, a relative velocity is created between the magnetic beads and the magnet, which results in a drag force acting on the beads. For the single-magnet configuration at slow tube velocities, such as the magnet-engaged speed (Figure 3(b)), the magnetic cluster experiences a shearing effect, and the cluster elongates along the tube wall. At the same speed in the two-magnet configuration (Figure 3(f)), the leading edge of the horizontal hourglass shape begins to flatten due to fluid drag but the overall structure is held in place by the concentrated magnetic field.

An increase in tube velocity shows the potential for mixing with a second magnet present. At a higher tube velocity, the single magnet configuration shows little difference from the tube moving at the much slower magnet-engaged speed (Figures 3(b) and 3(c)). With a second magnet present, the magnetic beads experience strong forces towards the closest tube wall. Immediately after stopping the tube (Figure 3(h)), the beads were much more dispersed throughout the solution. Two seconds after stopping the tube motion, the inertia resulting from the tube motion and the magnetic forces placed on the beads with two magnets results in a mixed bead solution. Alternatively, there is only a small improvement in the dispersion of the beads in the single-magnet system after stopping the tube motion (Figure 3(d) relative to Figure 3(h)). In the short time after the rapid tube motion, any improved dispersion of the beads with the single magnet configuration primarily results from the magnet "smearing" the beads along the side of the tube wall.

B. Rheology of biofluids

The stress-strain relationships measured for all of the pure biofluids, shown in Figure 4, are typical of non-Newtonian fluids. Sputum and blood are distinct from the other biofluids in Figure 4, while saliva and serum appear more similar to PBST. Inspection of the fitted power-law coefficients, shown in Table II, highlights these differences further.

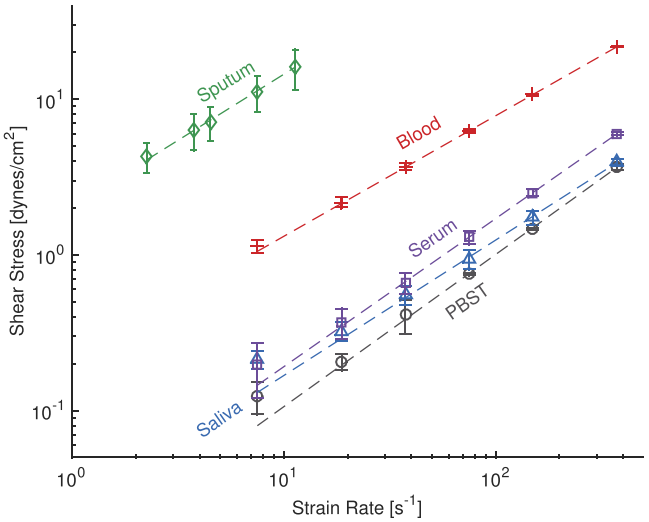

FIG. 4. Viscometer results for pure biofluids used in this study. The dashed lines are the fitted power-law relationships for each biofluid.

TABLE II. Fitted power-law coefficients, apparent viscosity for biofluids at a shear rate of 10 s^{-1}, and the diffusivity of HGFP in biofluids at their apparent viscosity calculated by Eq. (7). Biofluids with PBST were at a 1:1 (v/v) ratio.

	Flow consistency index (K)	Flow behavior index (n)	Apparent viscosity (Pa × s), $\dot{\gamma} = 10\ s^{-1}$	HGFP diffusivity in biofluid (m^2/s)
PBST	0.0112	0.9778	0.00106	7.1795×10^{-11}
Saliva	0.0227	0.8700	0.00168	4.5299×10^{-11}
Serum	0.0214	0.9515	0.00191	3.9844×10^{-11}
Blood	0.2214	0.7744	0.01317	5.7785×10^{-12}
Sputum	2.0460	0.8498	0.14478	5.2564×10^{-13}
Saliva:PBST	0.0127	0.9620	0.00116	6.5606×10^{-11}
Serum:PBST	0.0137	0.9673	0.00127	5.9923×10^{-11}
Blood:PBST	0.0361	0.9135	0.00295	2.5798×10^{-11}
Sputum:PBST	0.6712	0.7552	0.03820	1.9922×10^{-12}

The flow consistency index of a Newtonian fluid has a value of one; therefore, the flow consistency indices of more non-Newtonian fluids are further from unity. As all of the biofluids tested have flow behavior indices less than one, they are known as shear-thinning fluids; as the rate of shear that the fluid experiences increases, the apparent viscosity of the fluid decreases. At a shear rate of $10\,s^{-1}$, pure blood and pure sputum have apparent viscosities nearly one and two orders of magnitude larger than the other fluids, respectively.

After dilution into a 1:1 volume ratio of the less viscous PBST, all of the biofluids became more Newtonian, with the exception of sputum which had a slight decrease in its flow behavior index. For blood and sputum, this dilution resulted in a more than 50% decrease in their apparent viscosity. HGFP, with a hydrodynamic radius of 2.82 nm,[33] has a small diffusivity even in PBST. In sputum, the molecular diffusivity of HGFP decreases by nearly two orders of magnitude. Diluting the sputum with an equal volume of PBST still results in a molecular diffusivity of HGFP that is smaller than the molecular diffusivity of HGFP in any of the other pure biofluids.

C. Bulk fluid and bead transport

One of the advantages of pre-arrayed fluid cartridges is that they separate sequential processing steps and do not contaminate downstream chambers with fluid from the previous processing steps. Since an air valve separates the fluids, the only means for this contamination to occur is by bulk fluid transport. Our simulations and qualitative imaging have shown that the presence of a second magnet increases the contact between the magnetic beads and the surrounding fluid. This increase in available surface area offers the potential for larger volumes of fluid to be passively carried to the next chamber on the surface of individual beads or in the interstitial space of bead clusters. By replacing the HGFP with a non-binding fluorescent dye, we measured the passive fluid carryover in the two-magnet system to be nearly identical to that of the one-magnet system. Both magnet configurations passively brought over approximately 500 nl of fluid. There was no statistically significant difference between the volume of bulk fluid carried over with one magnet and two magnets.

To maximize biomarker capture, it is important to avoid bead loss. After quantifying the beads in the final chamber of each biofluid assay (Figure 5), there was no statistically significant difference between bead transport with the single magnet and the two-magnet configurations. In addition, there is no correlation between viscosity and bead transport. To this point, despite more than a 30-fold difference in apparent viscosity, sputum and PBST transported 77.48% and 79.14% of the magnetic beads to the final chamber in the two-magnet configuration, respectively. In most of the biofluids, regardless of magnetic configuration, more than 75% of the magnetic beads from the first chamber were delivered to the final chamber. The

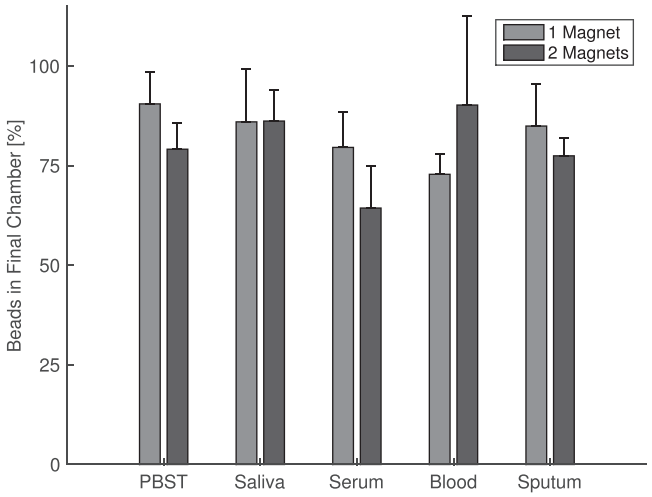

FIG. 5. Beads in the final chamber. Unpaired Student's T-Tests indicate that there is no statistically significant difference between the percentage of beads in the final chamber for a given biofluid using the 1-magnet system or the 2-magnet system.

only two exceptions to this were blood with a single magnet (72.84%) and serum with two magnets (64.37%).

D. Biomarker extraction and quantification in buffer

These experiments used HGFP in PBST and Cobalt-NTA surface functionalized magnetic beads to achieve a specific and rapid surface reaction. This model system served as a measure of the dispersion of beads throughout the fluid chamber as a function of magnetic configuration. The importance of convective dispersion of the beads throughout the fluid is highlighted in Figure 6 and compared to the two extremes of pure diffusion and readily available laboratory vortexing in a microcentrifuge tube. Vortexing the beads and the HGFP-buffer solution in a microcentrifuge tube for 7 min, the equivalent residence time of 5 mixing cycles in our assay tube processing, captured nearly 100% of the HGFP. By contrast, molecular diffusion for 28 min, the equivalent residence time of 25 cycles, resulted in only 8% of HGFP captured.

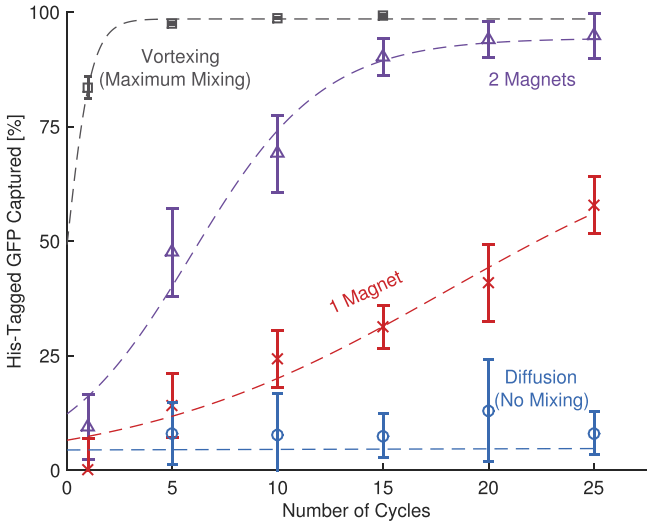

FIG. 6. HGFP extraction in PBST for varying number of cycles. The fitted lines are for a sigmoidal mixing curve (Eq. (8)) with fitted parameters shown in Table III.

TABLE III. Fit parameters for each mixing method (from Eq. (8)).

	p_∞ (%)	a (cycles^{-1})	n_0 (cycles)
Vortexing	98.53	1.715	2.22×10^{-14}
2 magnet mixing	94.34	0.3203	5.917
1 magnet mixing	78.51	0.1325	18.05
Diffusion	113.7	0.0028	1155

Magnetic mixing showed a strong dependence on the number of cycles. The presence of a second magnet increased HGFP capture across all of the number of cycles tested, when compared to the single magnet system. Mixing in microfluidic devices has been modeled by a sigmoidal function,[34] similar to that in the following equation:

$$P_{cap} = \frac{p_\infty}{1 + e^{-a(n_c - n_0)}}. \tag{8}$$

Applying this mixing function to the current mixing system, p_∞ is the maximum percentage of HGFP that can be captured, a is indicative of the steepness of the sigmoidal function, and n_0 is the number of cycles at which half of the HGFP has been captured. In a mass transfer context, p_∞ is the steady state fraction of HGFP that is bound from solution, a is related to the mass transfer coefficient, and n_0 is a time scale.

A sigmoidal function was fit to the data for the vortexing ($R^2 = 0.9896$), 2 magnet mixing ($R^2 = 0.9751$), and 1 magnet mixing ($R^2 = 0.9458$); it was a poor fit for diffusive mixing ($R^2 = 0.4426$). Excluding the values for diffusion, the p_∞ and a values were largest in the microcentrifuge tube vortexing, followed by the 2 magnet mixing, and then the 1-magnet mixing. The n_0 parameter followed the opposite trend; it was largest in the 1-magnet mixing, lower in the 2-magnet mixing, and smallest in the vortexing case.

E. Biomarker extraction in clinically relevant biomatrices

The mixing protocol with 25 cycles was tested in the presence of one and two magnets in the more clinically relevant biomatrices of blood, sputum, serum, and saliva. For each of these biofluids, the presence of the second magnet resulted in more protein being eluted from the surface of the beads than with a single magnet alone, presumably because more was captured. In buffer, the mean value of biomarker eluted with the one-magnet configuration was higher than the mean value of biomarker eluted with the two-magnet configuration, although this difference was not statistically significant. The largest difference between one magnet and two magnets was seen after 25 cycles of mixing in saliva; here the eluted HGFP concentration increased by 2.5-fold. Figure 7 shows that even in relatively low viscosity biomatrices, the two-magnet mixing approach improves bead-target interaction. Sputum, with its large apparent viscosity, significantly reduced HGFP capture, and there was not an appreciable amount of the biomarker eluted after 25 mixing cycles with only a single magnet in place. However, with a second magnet, more than 20% of the HGFP was recovered.

The elution of HGFP was fit to an exponential decay equation (Eq. (9)), and the best-fit parameters are shown in Figure 7

$$G = 100e^{-(b\mu)} + C. \tag{9}$$

The decay constant, b, was greater for a single magnet than for the two-magnet configuration. The best-fit constant term in Eq. (9), C, was found to be 0 for a single magnet, and 20.91 for the two-magnet system.

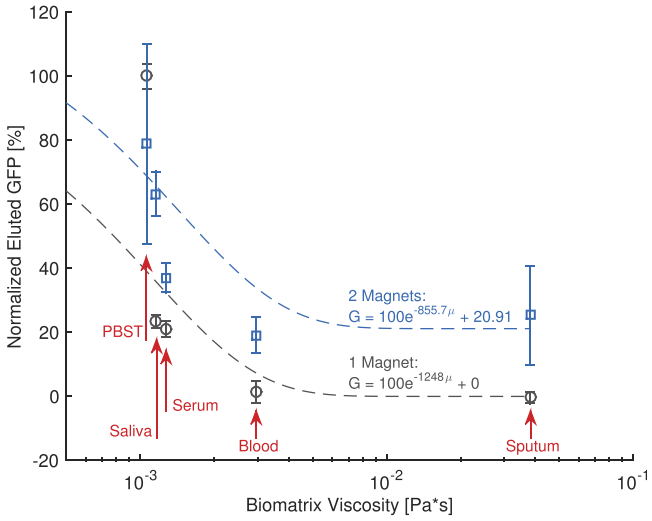

FIG. 7. Eluted HGFP after 25 passes through each biomatrix, normalized by the amount of HGFP eluted after 25 passes in PBST in the 1-magnet configuration. The lines are fit to an exponential decay equation (Eq. (9)).

IV. DISCUSSION

From our previous work using magnetic beads to capture biomarkers of infection, we know that the initial binding step where beads interact with the target biomarker is a major component of the overall assay time. In static fluids, where binding is diffusion-limited, the time for a biomolecule to diffuse over a characteristic length, L, is given by $t = L^2/D_{ab}$, where D_{ab} is the molecular diffusivity of the biomolecule. Biomolecule diffusivity will decrease proportionally with an increasing viscosity of the fluid, and our rheological measurements have allowed for the calculation of an effective diffusivity of HGFP in several biomatrices. For blood, our apparent viscosity is in agreement with rheological measurements taken at room temperature.[35,36] There is approximately a 2.5-fold increase in blood viscosity when the temperature decreases from physiological (37 °C) to room temperature (22 °C).[35] This magnifies the inefficiency of molecular diffusion in diagnostic devices, which are typically operated at ambient temperature. In large reaction chambers or in fluids with small diffusivities, a diffusion time on the order of days is prohibitively long for medical diagnostic tests. As such, there is a need for methods that improve bead-biomarker interactions and result in shorter binding steps.

To quantify the extent of mixing in the two-magnet and one-magnet systems, we used Cobalt-NTA surface functionalized magnetic beads that bind HGFP. Our results show that in buffer, the magnetic beads bind the target protein in fewer cycles using the two-magnet system. The fit parameters from Eq. (8) show that the two-magnet system has a larger a value, which indicates that HGFP is bound at a faster rate (in percent per cycle). The p_∞ parameter represents 50% of the final bound HGFP, and n_0 represents the number of cycles necessary to bind p_∞. Despite having a smaller p_∞, the single magnet system would take nearly 12 more mixing cycles to reach 50% of its p_∞. Given a sufficient amount of time, molecular diffusion alone would theoretically allow all of the mixing systems to reach 100% binding. Therefore, continuing the 1-magnet experiments to a larger number of mixing cycles would lead to a higher p_∞. However, the time required for more than 25 mixing cycles is beyond a practical amount of time for a diagnostic test. As well as the minimum mixing case of diffusion, we have compared our magnetic mixing strategies to a standard laboratory method for mixing beads in fluid samples: vortexing in a microcentrifuge tube. Vortexing represents an upper limit on the mixing that can be obtained using available laboratory procedures. Mixing in a microcentrifuge tube shows that after the equivalent of 5 assay-tube mixing cycles, nearly 100% of the HGFP is bound. While this illustrates that vortexing is an excellent means of dispersing beads throughout a fluid in a microcentrifuge tube, vortexing the pre-arrayed assay tube would result in

hydrodynamic instabilities that would combine the otherwise separated fluid chambers.[27] This re-iterates the importance of mixing strategies to improve the rate of target biomarker binding, and hence shorten processing times, in pre-arrayed microfluidic cassettes designed for off-the-shelf use.

In all of the clinically relevant biomatrices, more biomarker was eluted after mixing and extraction with the two-magnet configuration. Modeling the amount of protein captured and eluted as an exponential decay function implies that as viscosity increases, the mixing strategy will exponentially lose effectiveness. The decay parameter, b, is an indication of how rapidly this decrease will occur, and the baseline parameter, C, represents the amount of protein that could be recovered at very large viscosities. We have found that as biomatrix viscosity increases, the 1-magnet system captures and elutes less target biomarker than the 2-magnet system. In fact, the 1-magnet system did not capture the HGFP in the more viscous biomatrices, leading to a baseline parameter of 0. This is in contrast to the 2-magnet system, which had a baseline parameter of 20.91, indicating that even at large viscosities the increased dispersion of the magnetic beads improved protein capture. The two-magnet system shows improved performance in the less viscous clinical biofluids and maintains superior efficiency as biofluid viscosity increases. Still, these results would suggest that viscous biofluids should be pre-treated before sample processing to improve biomarker extraction efficiency.

With a single stationary magnet, mixing strategies in pre-arrayed fluid cartridges are limited to: magnet-engaged movement of a cluster of beads throughout a solution or magnet-engaged clustering of beads followed by gravitational settling. Our simulations and qualitative imaging show that the presence of a second magnet results in greater interaction between the magnetic beads and the surrounding fluid. The simulated magnetic force field vectors also indicate the potential for capitalizing on a new mixing modality, based on high velocity relative tube motion. This mixing strategy is based on the premises that with a second magnet present, there is less clumping of the magnetic beads, and if the beads are rapidly moved away from the magnets, there is improved bead dispersion throughout the tube and not just unidirectional translation. This agrees with the work by Long *et al.*, who found three distinct regimes in their study of the manipulation of droplets containing magnetic beads across a flat surface: steady droplet transport, magnet disengagement from the droplet, and magnetic bead extraction from the droplet.[37] While there are several distinctions between their work and our study, their force balance operating diagram is still applicable to our work. At the magnet-engaged tube speed, the magnetic force is greater than the drag force, and the magnetic beads remain captured. After the velocity is increased to the magnet-disengaged speed, the drag force is greater than the magnetic force, and the beads are disengaged from the magnet. As this occurs, the beads experience varying magnetic fields and magnetic field gradients with the two-magnet system that improves dispersion relative to the one-magnet system. We believe that most of the HGFP binding occurs during this dispersed stage. This addition of a second magnet, along with a rapid magnet-disengaging motion, is straightforward modifications that could improve the processing of other pre-arrayed microfluidic cassette designs.[16,17]

In addition to improving mixing, we have demonstrated that the addition of the second magnet does not alter the functionality of the surface tension valves, which is critical in multi-chamber processing applications. There is no statistically significant difference in the amount of fluid carried from one chamber to the next, regardless of the use of a single magnet or two magnets. Likewise, for the biofluids tested, there is no statistically significant difference between the number of beads that are transported to the final chamber for the 1-magnet and 2-magnet systems. Thus, the function of the surface tension valves remains unaffected with multiple magnets.

With further optimization, specifically of the magnetic field and the tube velocity, the overall function of the system can be improved. Ultimately, the amount of beads with bound biomarker that arrive in the final processing chamber will dictate the sensitivity of the assay. Our experiments have demonstrated that bead capture was consistent for a given biofluid, but leaves room for improvement. Varying the relative tube motion profile and the magnetic field has the potential to improve biomarker binding, as well as bead carryover to subsequent chambers.

While vortexing showed faster biomarker capture, it is not feasible for pre-arrayed diagnostic cartridges. In these types of devices, there must be a balance between assay time and assay precision, and the two-magnet system has the potential to improve both to the high levels seen with vortex mixing.

V. CONCLUSIONS

In magnetic-bead based biomarker extraction, strategies to disperse beads throughout the fluid are limited in the presence of a single magnet. The addition of a second magnet alters the magnetic field and presents new potential modalities for mixing. The relative motion between the magnetic beads and a pair of magnets results in superior interaction between the beads and the fluid compared to a single magnet configuration. This easy-to-implement modification can be utilized in pre-arrayed diagnostic assay cartridges to shorten assay times and improve efficacy in viscous patient samples.

ACKNOWLEDGMENTS

This work was supported in part by the Bill and Melinda Gates Foundation through the Grand Challenges in Global Health initiative (OPP 1028749). Thomas Scherr would like to acknowledge support from the Laboratories for Innovation in Global Health Technologies at Vanderbilt University.

APPENDIX: STATIC MAGNETIC SIMULATION THEORY

To determine the spatial magnetic field that arises due to the presence of the permanent magnets, the following equations were solved:

$$\mathbf{H} = -\nabla V_m, \tag{A1}$$

$$\nabla \cdot \mathbf{B} = 0. \tag{A2}$$

The liquid regions were modeled using the relative permeability constitutive relation

$$\mathbf{B} = \mu_0 \mu_r \mathbf{H}, \tag{A3}$$

while the magnets were given a remanent flux density of 0.6898 T

$$\mathbf{B} = \mu_0 \mu_r \mathbf{H} + \mathbf{B}_r. \tag{A4}$$

An insulation condition was chosen for the edges of the simulation domain

$$\boldsymbol{n} \cdot \mathbf{B} = 0. \tag{A5}$$

[1]M. A. M. Gijs, Microfluid. Nanofluid. **1**(1), 22–40 (2004).
[2]M. A. M. Gijs, F. Lacharme, and U. Lehmann, Chem. Rev. **110**(3), 1518–1563 (2010).
[3]Q. A. Pankhurst, J. Connolly, S. K. Jones, and J. Dobson, J. Phys. D: Appl. Phys. **36**(13), R167–R181 (2003).
[4]C. D. Chin, V. Linder, and S. K. Sia, Lab Chip **7**(1), 41–57 (2007).
[5]M. Rendl, T. Brandstetter, and J. Ruhe, Langmuir **30**(43), 12804–12811 (2014).
[6]H. A. Stone, A. D. Stroock, and A. Ajdari, Annu. Rev. Fluid Mech. **36**, 381–411 (2004).
[7]J. W. Choi, K. W. Oh, J. H. Thomas, W. R. Heineman, H. B. Halsall, J. H. Nevin, A. J. Helmicki, H. T. Henderson, and C. H. Ahn, Lab Chip **2**(1), 27–30 (2002).
[8]T. M. Squires and S. R. Quake, Rev. Mod. Phys. **77**(3), 977–1026 (2005).
[9]K. Zhang, Q. L. Liang, S. Ma, X. A. Mu, P. Hu, Y. M. Wang, and G. A. Luo, Lab Chip **9**(20), 2992–2999 (2009).
[10]D. J. Beebe, G. A. Mensing, and G. M. Walker, Annu. Rev. Biomed. Eng. **4**, 261–286 (2002).
[11]R. S. Sista, A. E. Eckhardt, V. Srinivasan, M. G. Pollack, S. Palanki, and V. K. Pamula, Lab Chip **8**(12), 2188–2196 (2008).
[12]B. P. Casavant, D. J. Guckenberger, D. J. Beebe, and S. M. Berry, Anal. Chem. **86**(13), 6355–6362 (2014).
[13]M. Shikida, K. Takayanagi, H. Honda, H. Ito, and K. Sato, J. Micromech. Microeng. **16**(9), 1875–1883 (2006).

[14]S. M. Berry, L. J. Maccoux, and D. J. Beebe, Anal. Chem. **84**(13), 5518–5523 (2012).
[15]L. Strotman, R. O'Connell, B. P. Casavant, S. M. Berry, J. M. Sperger, J. M. Lang, and D. J. Beebe, Anal. Chem. **85**(20), 9764–9770 (2013).
[16]B. P. Casavant, D. J. Guckenberger, S. M. Berry, J. T. Tokar, J. M. Lang, and D. J. Beebe, Lab Chip **13**(3), 391–396 (2013).
[17]S. M. Berry, E. T. Alarid, and D. J. Beebe, Lab Chip **11**(10), 1747–1753 (2011).
[18]A. Creecy, P. K. Russ, F. Solinas, D. W. Wright, and F. R. Haselton, PLoS One **10**(7), 1–14 (2015).
[19]K. Sur, S. M. McFall, E. T. Yeh, S. R. Jangam, M. A. Hayden, S. D. Stroupe, and D. M. Kelso, J. Mol. Diagn. **12**(5), 620–628 (2010).
[20]V. Linder, S. K. Sia, and G. M. Whitesides, Anal. Chem. **77**(1), 64–71 (2005).
[21]H. Bordelon, P. K. Russ, D. W. Wright, and F. R. Haselton, PLoS One **8**(7), 1–9 (2013).
[22]H. Bordelon, N. M. Adams, A. S. Klemm, P. K. Russ, J. V. Williams, H. K. Talbot, D. W. Wright, and F. R. Haselton, ACS Appl. Mater. Interfaces **3**(6), 2161–2168 (2011).
[23]M. Zimmermann, P. Hunziker, and E. Delamarche, Microfluid. Nanofluid. **5**(3), 395–402 (2008).
[24]S. Q. Wang, S. Tasoglu, P. Z. Chen, M. Chen, R. Akbas, S. Wach, C. I. Ozdemir, U. A. Gurkan, F. F. Giguel, D. R. Kuritzkes, and U. Demirci, Sci. Rep. - UK **4**, 1–9 (2014).
[25]S. Tanriverdi, L. J. Chen, and S. Q. Chen, J. Infect. Dis. **201**, S52–S58 (2010).
[26]A. L. Bitting, H. Bordelon, M. L. Baglia, K. M. Davis, A. E. Creecy, P. A. Short, L. E. Albert, A. V. Karhade, D. W. Wright, F. R. Haselton, and N. M. Adams, "Automated device for asynchronous extraction of RNA, DNA, or protein biomarkers from surrogate patient samples," J. Lab. Autom. (published online 2015).
[27]N. M. Adams, A. E. Creecy, C. E. Majors, B. A. Wariso, P. A. Short, D. W. Wright, and F. R. Haselton, Biomicrofluidics **7**(1), 14104 (2013).
[28]K. M. Davis, J. D. Swartz, F. R. Haselton, and D. W. Wright, Anal. Chem. **84**(14), 6136–6142 (2012).
[29]K. M. Davis, L. E. Gibson, F. R. Haselton, and D. W. Wright, Analyst **139**(12), 3026–3031 (2014).
[30]S. R. Subia, M. S. Ingber, L. A. Mondy, S. A. Altobelli, and A. L. Graham, J. Fluid Mech. **373**, 193–219 (1998).
[31]R. J. Phillips, R. C. Armstrong, R. A. Brown, A. L. Graham, and J. R. Abbott, Phys. Fluids A **4**(1), 30–40 (1992).
[32]N. N. Sanders, E. Van Rompaey, S. C. De Smedt, and J. Demeester, Am. J. Respir. Crit. Care Med. **164**(3), 486–493 (2001).
[33]O. Liarzi and B. L. Epel, Protoplasma **225**(1–2), 67–76 (2005).
[34]M. R. Bringer, C. J. Gerdts, H. Song, J. D. Tice, and R. F. Ismagilov, Philos. Trans. R. Soc. A **362**(1818), 1087–1104 (2004).
[35]P. W. Rand, E. Lacombe, H. E. Hunt, and W. H. Austin, J. Appl. Physiol. **19**(1), 117–122 (1964).
[36]D. M. Eckmann, S. Bowers, M. Stecker, and A. T. Cheung, Anesth. Analg. **91**(3), 539–545 (2000).
[37]Z. C. Long, A. M. Shetty, M. J. Solomon, and R. G. Larson, Lab Chip **9**(11), 1567–1575 (2009).